RSC Advances

PAPER

View Article Online
View Journal | View Issue

Check for updates

Cite this: *RSC Adv.*, 2023, **13**, 32217

Theoretical study of Ponceau S oxidation using the electro-Fenton process under optimal operational conditions

Yasmine Laftani, * Baylassane Chatib, Abdelghani Boussaoud and Mohsine Hachkar

Received 12th July 2023
Accepted 30th September 2023

DOI: 10.1039/d3ra04677j

rsc.li/rsc-advances

Electrochemical methods as one of the Advanced Oxidation Processes (AOPs) have been applied effectively to the degradation of recalcitrant organic molecules in aqueous solutions. In the present study, the performance of the electro-Fenton (EF) process on the oxidation of Ponceau S(PS) dye was studied. The experimental study performed at the optimal factors like the solution pH, the PS concentration and the ferrous ions dose provided 74.35% of PS degradation. The results, however, showed a decreased removal efficiency of PS when using sodium sulphate as the supporting electrolyte. From a theoretical point of view, the hydroxyl radical being an electron acceptor and the PS dye an electron donor, from a theoretical point of view, the hydroxyl radical being an electron acceptor and the PS dye an electron donor, furthermore, the nitrogen atom 2N being the most nucleophilic site of the PS dye with the most electrophilic site of the hydroxyl radical being the oxygen atom, the first stage of the reaction between PS and the hydroxyl radical was suggested.

Open Access Article. Published on 02 November 2023. Downloaded on 1/23/2025 9:21:11 AM.
This article is licensed under a Creative Commons Attribution-NonCommercial 3.0 Unported Licence.

1. Introduction

The textile industries are one of the most water-consuming sectors, estimated at several thousand cubic meters (m^3) per day.[1] Their effluents can be very coloured and resistant to biodegradation.[2,3] Consequently, they can cause a wide variety of environmental and health problems. Regarding synthetic dyes released in effluents from textile industries, azo dyes represent almost 50% of about 700 000 tons of dyes produced in the world.[4,5] As a di-azo dye, Ponceau S (PS), frequently detected in various water environments, is a kind of refractory organic matter that can put humans and other organisms in danger.[6,7]

Several technologies such as biodegradation, adsorption and oxidation methods have not yet shown success in degrading such refractory organics.[8] Depending on the nature and extent of the pollution, different processes can be employed for the purification of such effluents. Advanced oxidation processes (AOPs) are considered as high-efficiency physical–chemical processes due to their thermodynamic viability and capability to degrade or even mineralize a wide range of contaminants *via* the participation of free radicals,[9,10] mainly $HO^{\bullet}$ hydroxyl radicals.[11,12] The electro-Fenton (EF) process is a potentially effective AOP for treating several kinds of effluents.[1] There are notable advantages of electrochemistry, including energy efficiency, versatility and environmental suitability as the electrons and main-stream reagents are clean. Hence, by coupling electrochemistry with the Fenton process, the oxidation efficiency can be significantly improved.[13]

The electro-Fenton oxidation process involves either oxidizing Fe^{2+} or reducing Fe^{3+} electrochemically along with the simultaneous production of H_2O_2. The H_2O_2 is electrogenerated by the reduction of O_2 on the cathode, and then H_2O_2 reacts with Fe^{2+} to produce ferric ions, OH^- and hydroxyl radicals for the degradation of organics.[14,15] The molecular oxygen necessary for the production of hydrogen peroxide is regenerated at the anode by the oxidation of water.[16]

The electro-Fenton process can overcome the drawbacks of the traditional Fenton process, including the risk derived from storage and transportation of the concentrated H_2O_2, and the formation of large quantities of iron sludge. Meanwhile, due to the main performed reaction, it can avoid mass transfer limitations encountered during electrochemical oxidation. Moreover, the electro-Fenton process does not use any harmful and toxic materials; it is an environmentally friendly and low-cost method for treating wastewater.[17] However, the electro-Fenton process has been found to suffer from the low efficiency of Fe^{3+}/Fe^{2+} cycle and is limited to operating at conditions of low pH.[18]

Researchers have been using computational methods for achieving descriptions of molecular structures, spectroscopic properties and molecular reactivity.[19] Depending on the overall electronic character of the bond formation and/or bond breaking during the reaction, organic reactions can be categorised as non-polar or polar. Most organic molecules with

Laboratory of Process, Signals, Industrial Systems and Computer Science, Graduate School of Technology, Cadi Ayyad University, Morocco. E-mail: laftani90yasmine@gmail.com; Tel: +21-2639941253

© 2023 The Author(s). Published by the Royal Society of Chemistry

Open Access Article. Published on 02 November 2023. Downloaded on 1/23/2025 9:21:11 AM. This article is licensed under a Creative Commons Attribution-NonCommercial 3.0 Unported Licence.

polarised functional groups present a polar reactivity, which is characterised by a nucleophilic/electrophilic interaction. While electrophiles are molecules able to accept electron density during the reaction, nucleophiles are molecules able to donate electron density during the reaction. The electrophilic or nucleophilic power of a molecule is associated with its ability to exchange electron density during a reaction.[20]

In the current work, we applied electrochemical Fenton processes to the degradation of an aromatic pollutant, namely the PS dye, and investigated the reaction mechanism of the PS dye degradation using theoretical studies, namely density functional theory (DFT) with the DFT B3LYP calculation method and the 6-31G(d,p) basis set. The experimental studies were performed under optimal operating conditions.

2. Materials and methods

2.1. Materials

The PS dye, a tetrasodium salt of 3-hydroxy-4-({2-sulfo-4-[(4-sulfophenyl)-diazenyl]-phenyl}-diazenyl)-naphthalene-2,7-disulfonic acid, was purchased from Reactifs Ral. Hydrogen peroxide (H_2O_2, 50%) was obtained from Prochilabo. $FeSO_4 \cdot 7H_2O$ (99%) and H_2SO_4 (98%) were obtained from Sigma-Aldrich. NaOH was purchased from Scharlau.

All chemical reagents were of analytical grade. Synthetic solutions of PS dye were prepared with distilled water obtained using a GFL 2004 apparatus.

2.2. Experimental

The electrochemical treatment was carried out in an electrochemical cell, which consisted of a stirred reactor with two electrodes: vitreous carbon as the working electrode and platinum (Pt) as the anode. The current applied between the electrodes was produced using a current generator under 2.5 V of voltage.

The treated solutions were each kept stirred to avoid mass transport to/from the electrodes. The cell was filled with 25 mL of a solution containing 0.06 mM of PS at 25 °C. During each experiment, oxygen saturation was provided by using an air pump for 30 minutes. The solutions were each acidified with sulfuric acid (H_2SO_4) to avoid precipitation of ferric ions as hydroxides, and a pH meter (Hach Sension+) was used to measure the pH of the solutions. Samples with volumes of 2 mL were taken at regular intervals and analysed to evaluate the variation of the residual PS dye dose.

2.3. Analytical methods

UV-visible spectra of PS diazo dye were recorded from 200 to 800 nm using a UV-visible spectrophotometer (Rayleigh UV-1800) with a spectrometric quartz cell (1 cm path length). The maximum absorbance wavelength (λ_{max}) of the PS dye could be found at 520 nm. The obtained data were analysed using Excel software.

The PS disappearance efficiency was calculated using the equation

$$\%\ \text{Disappearance efficiency} = \left(\frac{A_t - A_0}{A_0}\right) \times 100 \quad (1)$$

where A_0 is the initial absorption of PS, and A_t is the absorption of PS at reaction time t.

2.4. Theoretical

All calculations were optimized using the B3LYP (Becke – 3 parameters – Lee Yang Parr) functional with the standard 6-31G(d) basis set. All computations were carried out with Gaussian 09 software. Combined with the 6-31G(d) basis set, B3LYP has become the method of choice for efficient and accurate computation of most chemical properties. It is known for its relatively high accuracy in predicting molecular structures, energies, and properties of a wide range of chemical systems including organic, inorganic, and biological molecules. B3LYP has played a crucial role in predicting reaction mechanisms, electronic structures, and spectroscopic properties. Its accuracy and versatility make it an appreciated tool in these areas.[21]

Furthermore, 6-31G is known for being a reasonably accurate and computationally efficient basis set for a wide range of molecular systems, making it a popular choice for many applications.[20]

3. Results and discussion

3.1. Degradation of PS dye using the EF process

3.1.1. Choice of the cathode. A comparative study of PS dye degradation using electro-Fenton process was done by changing the nature of the cathode. This experiment was performed using an initial PS concentration of 0.06 mM, 0.06 mM of Fe^{2+} and a pH of 3.34. The obtained results are shown in Table 1.

When using the vitreous carbon cathode, a PS dye degradation efficiency of 74.35% was achieved. This cathode having also been shown to display technologically important characteristics such as high hydrogen overpotential, good conductivity, strong chemical resistance, and a smooth surface to which gas and dirt do not easily adhere,[28] it was used for the rest of this work.

3.1.2. Effect of the supporting electrolyte. In order to evaluate the impact of the supporting electrolyte on the PS dye degradation efficiency using the EF process, an investigation was carried out using Na_2SO_4 and NaCl solutions. For each experiment, the two electrodes were immersed in 25 mL of solution saturated with O_2 for 30 minutes, and a time plot of the resulting absorbance was drawn as shown in Fig. 1.

Table 1 Effect of the nature of the cathode on the PS degradation using the EF process

PS degradation efficiency (%)	
Graphite carbon electrode	Vitreous carbon electrode
17.93%	74.35%

© 2023 The Author(s). Published by the Royal Society of Chemistry

Open Access Article. Published on 02 November 2023. Downloaded on 1/23/2025 9:21:11 AM.
This article is licensed under a Creative Commons Attribution-NonCommercial 3.0 Unported Licence.

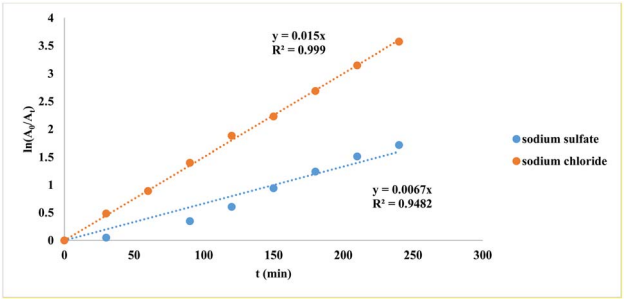

Fig. 1 Effect of the supporting electrolyte on the PS dye degradation using the EF process. Experimental conditions: [PS] = 0.06 mM; [Fe^{2+}] = 0.12 mM; [supporting electrolyte] = 0.2 mM; T = 25 °C; pH = 3.34.

Na_2SO_4 was tested instead as the supporting electrolyte to avoid the effects of Cl_2 and ClO^- generated at the anode when using NaCl. However, the use of Na_2SO_4 might have led to a passivation of the platinum electrode in the current work. NaCl showed the apparent advantage of increasing the solution conductivity during electrolysis and hence increasing the PS degradation efficiency.

3.2. Theoretical study

Many investigations have confirmed hydroxyl radicals to be the primary active substance for oxidizing PS dye. In order to elucidate the first step of the mechanism of the reaction between the PS dye and the hydroxyl radicals, a pathway based on DFT concepts was modelled. This approach in general allows access to global and local parameters to justify and predict the chemoselectivity and regioselectivity of the attack of reactive species on a substrate.[22]

3.2.1. Molecular geometry. The global electrophilicity ω index encompasses the tendency of an electrophile to acquire an extra amount of electron density, given by μ, and the resistance of a molecule to exchange electron density with the environment, given by η.[23]

The global electrophilicity descriptor (ω) is given using the expression

$$\omega = (\mu^2/2\eta) \quad (2)$$

where μ is the electronic chemical potential and η is the chemical hardness. Chemical softness (S) has also been used, as the inverse of the chemical hardness η, following the equation

$$S = (1/\eta). \quad (3)$$

Using the theorem developed by Koopmans and Kohn–Sham, both quantities may be approached in terms of frontier molecular orbitals, namely the highest occupied molecular orbital (HOMO) and lowest unoccupied molecular orbital (LUMO), using the equations

$$\mu = (E_{HOMO} + E_{LUMO})/2 \quad (4)$$

and

$$\eta = (E_{LUMO} - E_{HOMO})/2. \quad (5)$$

In 2008, an empirical (relative) nucleophilicity N index for closed-shell organic molecules based on the HOMO energies, obtained within the Kohn–Sham theorem, was proposed[24]—with this index defined using the equation

$$N = E_{HOMO}(\text{nucleophile}) - E_{HOMO}(\text{TCE}), \quad (6)$$

where tetracyanoethylene (TCE) presents the lowest HOMO energy of molecules investigated in the context of polar organic reactions.[23] The optimised PS dye structure with numbering of atoms obtained from GaussView software is shown in Fig. 2.

3.2.2. Global and local reactivity descriptors. The study of the reactivity descriptors is a powerful method used to understand the reactivity between polar species. The values obtained for the global descriptors of the PS dye and the hydroxyl radicals are listed in Tables 2 and 3, respectively.

(a). Global reactivity descriptors. No electron density exchange occurs during non-polar organic reactions involving neutral radical species. However, certain substitutions in the radical species may favour the occurrence of electron density exchange, thereby determining the chemical reactivity of these radical species.[6] Consequently, a set of DFT reactivity indices have recently been proposed for the study of the reactivity of free radicals. The global nucleophilicity N^0 of free radicals is presented by the equation using the equation

$$N^0 = E^{\alpha,0}_{HOMO}(\text{nucleophile}) - E^{\alpha,0}_{HOMO}(\text{DCM}), \quad (7)$$

where the dicyanomethyl (DCM) radical is taken as a reference to define a positive scale of global nucleophilicity of radicals. Table 3 presents $E^{\alpha,0}_{HOMO}$, $E^{\beta,0}_{HOMO}$, $E^{\alpha,0}_{LOMO}$, $E^{\beta,0}_{LOMO}$ energies, chemical potential μ, chemical hardness η, softness $S°$, global electrophilicity $\omega°$ and dipole moment μ (D) of the hydroxyl radicals.

A higher value of ω indicates a more electrophilic agent. The PS molecule was determined to have a global electrophilicity index (ω) of 3.533391 eV, compared to the value of the hydroxyl radical ($\omega° = 5.87$ eV), indicating a role as a nucleophile agent played by the PS dye and an electrophile role played by the hydroxyl radical.

A low chemical potential (high electronegativity) is associated with a good electrophile. The values of the calculated chemical potentials and those of the hardness were calculated to be $\mu = -4.457944$ eV and $\eta = 2.812208$ eV for PS and $\mu° = -7.40$ eV and $\eta° = 4.67$ eV for the hydroxyl radical, in agreement with the above results.

The reaction between the most electrophilic centre of an electrophilic reactant and the most nucleophilic centre of a nucleophilic reactant is the most important step of the reaction pathway during a reaction involving asymmetric reactants. Note that in the Fukui (HOMO and LUMO) frontier orbital approximation, a smaller HOMO–LUMO separation indicates a stronger interaction and a more favoured reaction.

(b). Local reactivity descriptors. In general in a local reactivity study, the Parr functions P_k^+ and P_k^- are essential tools for

Open Access Article. Published on 02 November 2023. Downloaded on 1/23/2025 9:21:11 AM.
This article is licensed under a Creative Commons Attribution-NonCommercial 3.0 Unported Licence.

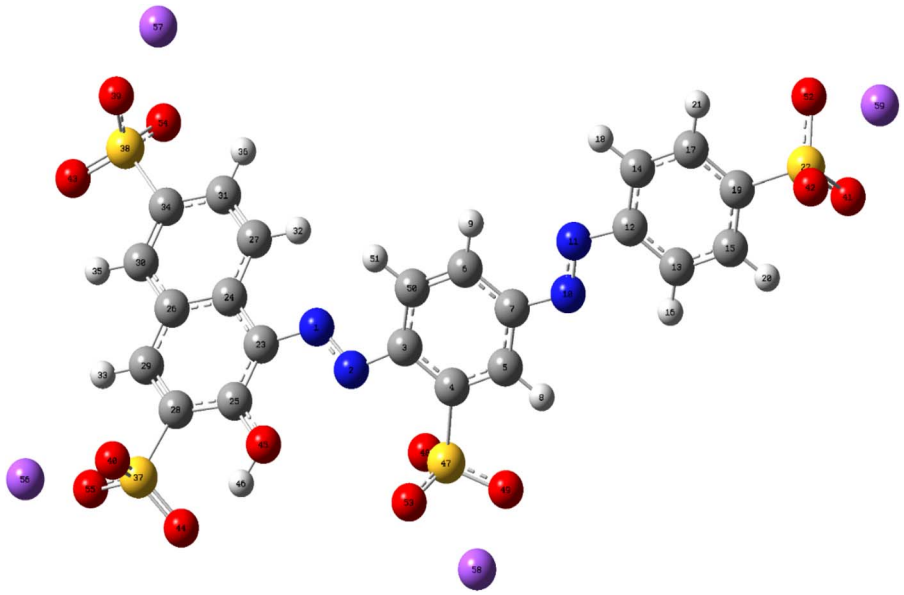

Fig. 2 Depiction of the three-dimensional molecular structure of the Ponceau S molecule optimized using Gaussian software.

Table 2 E_{HOMO} and E_{LUMO} energies, chemical potential μ, chemical hardness η, softness S, electrophilicity index ω, nucleophilicity N and dipole moment of the PS dye

E_{HOMO} (eV)	−5.864048
E_{LUMO} (eV)	−3.05184
μ	−4.457944
η (eV)	2.812208
ω (eV)	3.533391
N	3.130448
Dipole moment (debye)	7.4105
S	0.355592

Table 3 $E^{\alpha,0}_{HOMO}$, $E^{\beta,0}_{HOMO}$, $E^{\alpha,0}_{LOMO}$, $E^{\beta,0}_{LOMO}$ energies, chemical potential μ, chemical hardness η, softness $S°$, electrophilicity index $\omega°$ and dipole moment μ of the OH˙

$E^{\alpha,0}_{HOMO}$	−9.74
$E^{\beta,0}_{HOMO}$	−9.00
$E^{\alpha,0}_{LOMO}$	−1.21
$E^{\beta,0}_{LOMO}$	−5.07
$\mu°$	−7.40
$\eta°$	4.67
$S°$	0.21
$\omega°$	5.87
N^0	—
Dipole moment	2.07

characterizing the most electrophilic and nucleophilic centres of the reactants involved in a polar reaction process, and for subsequently explaining any regioselectivity.[25]

Recent studies of polar cycloaddition reactions have shown that the most favourable regioisomeric channel is that involving the bond formation between the most electrophilic and most nucleophilic centres of the reagents. Consequently, it is desirable to have local reactivity indices able to characterise these relevant centres in organic molecules.

Remarkably, analysis of the atomic spin density (ASD) at the radical cation and the radical anion gives a picture of the distribution of the electron density in the electrophile and the nucleophile when they approach each other during the progress of the reaction.[26]

In 2014, Domingo proposed the Parr functions $P(r)$, which are given by the equations

$$P_k^- = \rho_s^{rc} \text{ for electrophilic attacks} \quad (8)$$

and

$$P_k^+ = \rho_s^{ra} \text{ for nucleophilic attacks,} \quad (9)$$

where ρ_s^{rc} is the ASD at the k atom of the radical cation of a considered molecule and ρ_s^{ra} is the ASD at the k atom of the radical anion.[27] The results are shown in Table 4.

The local radical Parr function P_k^0 is defined as

$$P_k^0 = \rho_{sk}, \quad (10)$$

where ρ_{sk} is the ASD at site k of the free radicals. The local electrophilicity ω_k^0 and nucleophilicity N_k^0 descriptors can be obtained by using the equations

$$\omega_k^0 = \omega^0 P_k^0 \quad (11)$$

and

$$N_k^0 = N^0 P_k^0. \quad (12)$$

The analysis of the Parr functions of the PS dye indicated the 2N atom ($N_{2N} = 0.529$ eV) to be the most nucleophilic centre of this molecule. On the other hand, the Parr function analysis of

© 2023 The Author(s). Published by the Royal Society of Chemistry

Open Access Article. Published on 02 November 2023. Downloaded on 1/23/2025 9:21:11 AM.
This article is licensed under a Creative Commons Attribution-NonCommercial 3.0 Unported Licence.

Table 4 Electrophilic P_k^+ and nucleophilic P_k^+ Parr functions, local electrophilicity ω_k and the local nucleophilicity N_k descriptor of PS dye

Atom	P_k^+	P_k^+	ω_k	N_k
1 N	0.050112	0.190216	0.672107632	0.15687301
2 N	**0.169089**	**0.047884**	**0.169192927**	**0.529324322**
3 C	0.00261	0.092006	0.325093235	0.008170469
4 C	0.068599	0.019359	0.06840293	0.214745602
5 C	−0.040773	0.009958	0.035185514	−0.127637756
6 C	−0.033596	0.054368	0.192103439	−0.105170531
7 C	0.112171	0.039881	0.140915194	0.351145483
8 H	0.001281	−0.000759	−0.002681844	0.004010104
9 H	0.00097	−0.002899	−0.010243302	0.003036535
10 N	−0.040637	0.083247	0.294144257	−0.127212015
11 N	0.061533	0.206282	0.728875103	0.192625857
12 C	−0.007344	−0.037652	−0.133039264	−0.02299001
13 C	0.028599	0.082266	0.290678	0.089527682
14 C	0.030137	0.063158	0.223161952	0.094342311
15 C	−0.016321	−0.041681	−0.147275299	−0.051092042
16 H	−0.001152	−0.003941	−0.013925097	−0.003606276
17 C	−0.017562	−0.031342	−0.110743562	−0.054976928
18 H	−0.001304	−0.003053	−0.010787445	−0.004082104
19 C	0.040118	0.084638	0.299059205	0.125587313
20 H	0.00054	0.001476	0.005215286	0.001690442
21 H	0.000586	0.001061	0.003748929	0.001834443
22 S	−0.002229	−0.000179	−0.000632477	−0.006977769
23 C	0.181536	−0.063465	−0.224246703	0.568289008
24 C	−0.054631	0.055936	0.197643797	−0.171019505
25 C	0.087416	0.091947	0.324884765	0.273651242
26 C	−0.005565	−0.039358	−0.13906723	−0.017420943
27 C	0.096312	−0.028065	−0.099164638	0.301499708
28 C	−0.046193	−0.041896	−0.148034978	−0.144604784
29 C	0.108007	0.126196	0.445899897	0.338110297
30 C	0.036175	0.030762	0.108694195	0.113243956
31 C	−0.01274	0.036523	0.129050064	−0.039881908
32 H	−0.003546	0.0005	0.001766696	−0.011100569
33 H	−0.004312	−0.005815	−0.020546673	−0.013498492
34 C	0.050838	−0.024772	−0.087529179	0.159145715
35 H	−0.001405	−0.001271	−0.004490941	−0.004398279
36 H	0.000092	−0.001662	−0.005872497	0.000288001
37 S	0.001359	0.000393	0.001388623	0.004254279
38 S	−0.003368	0.000384	0.001356822	−0.010543349
39 O	0.00536	−0.000789	−0.002787846	0.016779201
40 O	−0.000489	−0.001128	−0.003985666	−0.001530789
41 O	0.001448	0.001393	0.004922015	0.004532889
42 O	0.003904	0.003645	0.012879213	0.012221269
43 O	0.002754	−0.000219	−0.000773813	0.008621254
44 O	−0.000154	−0.000621	−0.002194236	−0.000482089
45 O	0.088401	0.020142	0.071169575	0.276734734
46 H	−0.002092	−0.000542	−0.001915098	−0.006548897
47 S	−0.004888	0.000398	0.00140629	−0.01530163
48 O	0.007007	0.001361	0.004808946	0.021935049
49 O	−0.000279	0.000608	0.002148302	−0.000873395
50 C	0.058706	−0.01584	−0.055968924	0.18377608
51 H	−0.002461	0.000227	0.00080208	−0.007704033
52 O	0.001584	0.00131	0.004628743	0.00495863
53 O	0.003464	0.000422	0.001491091	0.010843872
54 O	0.003123	−0.000476	−0.001681894	0.009776389
55 O	−0.000418	−0.000569	−0.0020105	−0.001308527
56 Na	0.000051	0.000267	0.000943416	0.000159653
57 Na	−0.000159	0.00007	0.000247337	−0.000497741
58 Na	−0.000195	0.00004	0.000141336	−0.000610437
59 Na	−0.000072	−0.000333	−0.001176619	−0.000225392

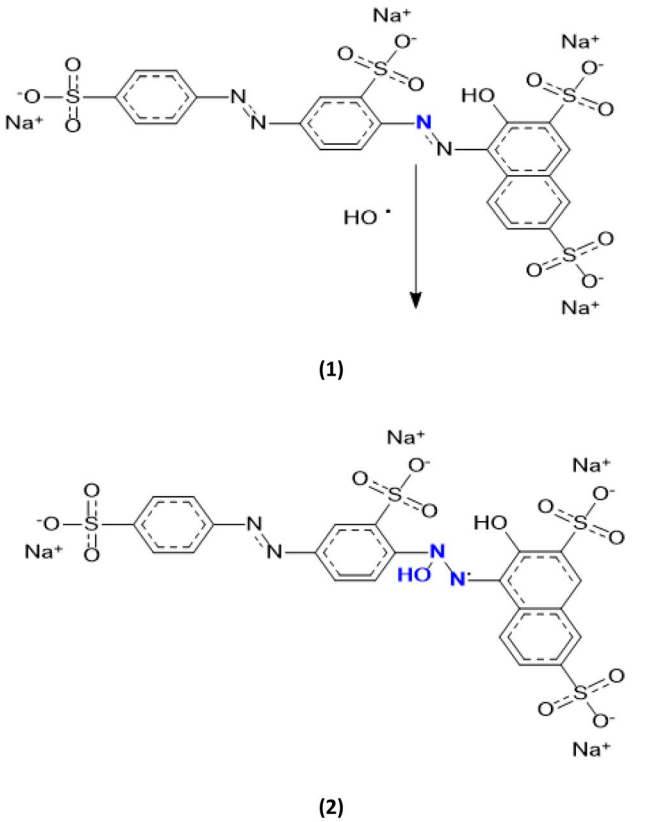

Fig. 3 Structural depictions showing the first mechanistic step proposed for the formation of the final compound (2) from the initial compound (1).

the hydroxyl radical indicated the oxygen atom (6.02 eV) to be the centre concentrating the local electrophilicity of this species.

Due to the hydroxyl radicals being electrophilic species, the dye hydroxylation would only take place at electron-rich sites, such as amino groups or those of the azo bond.

According to the literature, 60% of electrophilic attack reactions involving azo-containing compounds start with an addition onto the double bond of the azo group. The addition of hydroxyl radicals to the azo double bond could be considered as the first step in the degradation process. Once the –N═N– bond has been broken, the aromatic compounds can in turn be attacked by hydroxyl radicals.

The diazinyl group was confirmed, based on analysis of the regioselectivity indicators, to be the most nucleophilic centre of PS dye, with this centre first attacked by the hydroxyl radicals.

Thus, the most favourable electrophilic/nucleophilic interaction would be between the 2*N* nucleophilic centre of PS and the O electrophilic centre of the hydroxyl radicals and which would give rise to the compound (2) presented in Fig. 3.

4. Conclusion

The combination of chemical and electrochemical procedures is considered to be a good alternative to water treatment. At the optimized conditions, PS dye was removed at an efficiency of

Open Access Article. Published on 02 November 2023. Downloaded on 1/23/2025 9:21:11 AM. This article is licensed under a Creative Commons Attribution-NonCommercial 3.0 Unported Licence.

74.35%. Under the optimized conditions, the maximum degradation of PS dye was obtained by using sodium chloride as a supporting electrolyte.

Theoretical DFT calculation estimating the global and local reactivity indices demonstrated an electron donor behaviour displayed by the PS dye and an electron acceptor behaviour displayed by the hydroxyl radical. An analysis involving Parr functions indicated the local attack to be between nitrogen atom 2*N* of the PS dye and the oxygen atom of hydroxyl radical.

Conflicts of interest

There are no conflicts to declare.

References

1 B. Louhichi, F. Gaied, K. Mansouri and M. R. Jeday, *Chem. Eng. J.*, 2021, **427**, 131735.
2 Y. Laftani, A. Boussaoud, B. Chatib, M. El Makhfouk, M. Hachkar and M. Khayar, *Maced. J. Chem. Chem. Eng.*, 2019, **38**, 197.
3 B. Chatib, Y. Laftani, M. Khayar, M. El Makhfouk, M. Hachkar and A. Boussaoud, *Iran. J. Chem. Chem. Eng.*, 2021, **40**, 111–121.
4 N. Bougdour, A. Sennaoui, I. Bakas and A. Assabbane, *Sci. Technol. Adv. Mater.*, 2018, 1–9.
5 N. P. Tantak and S. Chaudhari, *J. Hazard. Mater.*, 2006, **136**, 698–705.
6 F. Z. Ankouri, H. Lamkhanter, A. Jaafar, Z. Lakbaibi and H. Mountacer, *Chem. Afr.*, 2023, **6**, 1495–1513, DOI: **10.1007/s42250-022-00579-y**.
7 M. Behrouzeh, *et al.* , *Arabian J. Chem.*, 2022, **15**, 104229, DOI: **10.1016/j.arabjc.2022.104229**.
8 Z. He, C. Gao, M. Qian, Y. Shi, J. Chen and S. Song, *Ind. Eng. Chem. Res.*, 2014, **53**, 3435–3447.
9 Y. Laftani, B. Chatib, A. Boussaoud, M. El Makhfouk, M. Hachkar and M. Khayar, *Water Sci. Technol.*, 2019, **80**, 1731–1739, DOI: **10.2166/wst.2019.424**.
10 Y. Laftani, B. Chatib, A. Boussaoud, M. Hachkar and M. El Makhfouk, *Water Qual. Res. J.*, 2022, 1–16.
11 Y. Laftani, A. Boussaoud, B. Chatib, M. Hachkar, M. El Makhfouk and M. Khayar, *Environ. Eng. Res.*, 2021, **27**, 210002.
12 M. A. Quiroz, E. R. Bandala and C. A. Martínez-huitle, Pesticides, in *Advanced Oxidation Processes (AOPs) for Removal of Pesticides from Aqueous Media*, 2007.
13 R. Javaid and U. Y. Qazi, *Int. J. Environ. Res. Public Health*, 2019, **16**, 1–27.
14 E. Brillas, M. Á. Baños, M. Skoumal, P. L. Cabot, J. A. Garrido and R. M. Rodríguez, *Chemosphere*, 2007, **68**, 199–209.
15 Y. Laftani, *Procédés de dépollution par oxydation avancée: cinetique & planification experimentale-cas du colorant ponceau S*, Cadi Ayyad University, 2021.
16 J. Li, Y. Li, Z. Xiong, G. Yao and B. Lai, *Chin. Chem. Lett.*, 2019, **30**, 2139–2146.
17 A. R. Rahmani, A. Shabanloo, J. Mehralipou, M. Fazlzadeh and Y. Poureshgh, *Res. J. Environ. Sci.*, 2015, **9**, 332–341.
18 D. Li, T. Zheng, J. Yu, H. He, W. Shi and J. Ma, *J. Ind. Eng. Chem.*, 2022, **105**, 405–413.
19 A. Jaafar, *et al.*, *Res. J. Chem. Environ.*, 2021, **25**, 74–78.
20 L. R. Domingo, P. Pe and J. A. Saez, *RCS Adv.*, 2013, 1486–1494.
21 K. Raghavachari, *J. Chem. Phys.*, 2000, 361–363.
22 H. Chermette, *J. Comput. Chem.*, 1999, **20**, 129–154.
23 L. R. Domingo and P. Pérez, *Org. Biomol. Chem.*, 2011, **9**, 7168–7175.
24 L. R. Domingo, M. Ríos-gutiérrez and P. Pérez, *Molecules*, 2016, **21**(6), 7482016.
25 A. Jaafar, *et al.*, *J. Chem. Res.*, 2019, **2**, 53–61.
26 P. Caregnato, *et al.*, *J. Phys. Chem. A*, 2008, **112**, 1188–1194.
27 S. Singireddy, *et al.*, *Origins Life Evol. Biospheres*, 2012, **42**, 275–294.
28 J. M. Friedrich, C. Ponce-de-León, G. W. Reade and F. C. Walsh, *J. Electroanal. Chem*, 2004, **561**, 203–217.

© 2023 The Author(s). Published by the Royal Society of Chemistry